Orientations of Tyr 21 and Tyr 24 in the Capsid of Filamentous Virus Ff Determined by Polarized Raman Spectroscopy[†,‡]

Masamichi Tsuboi,[§,||] Koichi Ushizawa,[⊥] Koji Nakamura,[§,@] James M. Benevides,[§] Stacy A. Overman,[§] and George J. Thomas, Jr.*[,§]

Division of Cell Biology and Biophysics, School of Biological Sciences, University of Missouri−Kansas City, Kansas City, Missouri 64110, Department of Fundamental Science, Iwaki-Meisei University, Iwaki, Fukushima 970-8551, Japan, and National Institute for Research in Inorganic Materials, 1-1 Namiki, Tsukuba, Ibaraki 305-0044, Japan

Received August 15, 2000; Revised Manuscript Received November 28, 2000

ABSTRACT: The capsid of filamentous virus Ff is assembled from ∼2750 copies of a 50-residue α-helical subunit, the two tyrosines of which (Tyr 21 and Tyr 24) are located within a hydrophobic sequence that constitutes the subunit interface. We have determined the side chain orientations of Tyr 21 and Tyr 24 by polarized Raman microspectroscopy of oriented Ff fibers, utilizing a novel experimental approach that combines site-specific mutation and residue-specific deuteration of capsid subunits. The polarized Raman signature of Tyr 21 was obtained by incorporating $C^{\delta 1}$,$C^{\delta 2}$,$C^{\epsilon 1}$,$C^{\epsilon 2}$-tetradeuteriotyrosine at position 21 in an Ff mutant in which Tyr 24 is replaced with methionine. Similarly, the polarized Raman signature of Tyr 24 was obtained by incorporating $C^{\delta 1}$,$C^{\delta 2}$,$C^{\epsilon 1}$,$C^{\epsilon 2}$-tetradeuteriotyrosine at position 24 in the analogous Tyr 21 → Met mutant. Polarizations of the corresponding C−D stretching bands in the 2200−2400 cm^{-1} interval of the Raman spectrum were measured and interpreted using tensors transferred from a polarized Raman analysis of L-tyrosine-2,3,5,6-d_4 single crystals. Polarized Raman analysis was extended to the bands of Ff near 642 and 855 cm^{-1}, which originate from vibrational modes of the tyrosine phenolic ring. The results indicate the following: (i) For both Tyr 21 and Tyr 24, the phenolic 2-fold axis (C^1-C^4 line) is inclined at 41 ± 5° from the virion axis and the normal to the plane of the phenolic ring is inclined at 71 ± 5° from the virion axis; (ii) the mutation of Tyr 24, but not the mutation of Tyr 21, perturbs Raman markers of the subunit tryptophan (Trp 26), suggesting interdependence of Tyr 24 and Trp 26 orientations in native Ff; and (iii) polarization anisotropies observed for Raman markers of Ff DNA bases are unperturbed by mutation of either Tyr 21 or Tyr 24, indicating that nonrandom base orientations of packaged Ff DNA are independent of the mutation of either Tyr 21 or Tyr 24. A molecular model consistent with these findings is proposed.

Bacteriophages fd, f1, and M13 are structurally identical members of the Ff group of filamentous viruses infecting F^+ strains of *Escherichia coli*. The cylindrical Ff filament (∼880 nm in length × ∼6 nm in diameter) contains a covalently closed and single-stranded (ss) DNA genome of 6410 nucleotides, sheathed by ∼2750 copies of a 50-residue α-helical subunit (pVIII) and a few copies of minor proteins at the filament ends. The pVIII sequence (AEGDDPAKAA FDSLQASATE YIGYAWAMVV VIVGATIGIK LFKKFTS-KAS) is identical among all members of the Ff class, except for the replacement of Asp with Asn at position 12 in M13. Further details of the genetics and assembly mechanism of Ff are given in various reviews (*1*−*4*).

The structure of the native Ff assembly has been studied by methods of solution and fiber spectroscopy and fiber X-ray diffraction (*5*−*24*), which collectively provide many details about pVIII main chain and side chain conformations, subunit orientation, and filament architecture. Overall, the results show that the ssDNA core of Ff is coated by a

† The support of this research by NIH Grant GM50776 is gratefully acknowledged.

‡ Paper LXXV in the series Structural Studies of Viruses by Raman Spectroscopy.

* To whom correspondence should be addressed. Telephone: (816) 235-5247. Fax: (816) 235-1503. E-mail: thomasgj@umkc.edu.

§ University of Missouri−Kansas City.

|| Iwaki-Meisei University.

⊥ National Institute for Research in Inorganic Materials.

@ Present address: Department of Physiology, Gifu University School of Medicine, Gifu, Japan.

[1] Abbreviations: Ff, class I filamentous virus, including strains fd, f1, and M13; pVIII, major coat protein of Ff; fd($2Y_{d4}$), fd in which both Tyr 21 and Tyr 24 are deuterium-labeled at $C^{\delta 1}$, $C^{\delta 2}$, $C^{\epsilon 1}$, and $C^{\epsilon 2}$; f1(Y21M), mutant f1 in which Tyr 21 is replaced with Met; f1-(Y24M), mutant f1 in which Tyr 24 is replaced with Met; f1(Y21M/$Y24_{d4}$), mutant f1 in which Tyr 21 is replaced with Met and Tyr 24 is deuterium-labeled at $C^{\delta 1}$, $C^{\delta 2}$, $C^{\epsilon 1}$, and $C^{\epsilon 2}$; f1(Y24M/$Y21_{d4}$), mutant f1 in which Tyr 24 is replaced with Met and Tyr 21 is deuterium-labeled at $C^{\delta 1}$, $C^{\delta 2}$, $C^{\epsilon 1}$, and $C^{\epsilon 2}$; ss, single-stranded; RLID, Raman linear intensity difference; UVRR, ultraviolet-resonance Raman; θ and χ, Eulerian angles defining the orientation of Raman tensor coordinates (x, y, z) with respect to laboratory coordinates (a, b, c); χ^1, side chain torsion angle defined by atoms N, C^α, C^β, and C^γ of tyrosine; χ^2, side chain torsion angle defined by atoms C^α, C^β, C^γ, and C^δ of tyrosine; $\chi^{2,1}$, side chain torsion angle defined by atoms C^α, C^β, C^γ, and $C^{\delta 1}$ of tryptophan.

10.1021/bi001936n CCC: $20.00
Published on Web 01/10/2001

superhelical array of pVIII subunits arranged with 5-fold rotational symmetry and an approximately 2-fold screw axis, and that the pVIII subunit is a continuous α-helix tilted at an average angle of approximately 16° from the virion axis.

Although atomic details of the coat protein cannot be determined directly by fiber X-ray diffraction, a molecular model has been proposed that is consistent with the diffraction data (Protein Data Bank entry 1IFJ) (*16*). However, the conformations of key aromatic side chains of pVIII (notably, Tyr 21, Tyr 24, and Trp 26) have been shown by methods of polarized Raman spectroscopy of oriented fibers (*17*) and ultraviolet-resonance Raman (UVRR) linear intensity difference (LID) spectroscopy of flow-oriented solutions (*18*, *21*) to differ in detail from the proposed model. For example, in determinations of the Trp 26 indolyl orientation by both RLID (solution) and polarized Raman (fiber) methods, the indolyl plane is found to be inclined at a small angle from the virion axis, such that the pseudo-2-fold axis of the ring forms an angle of ∼37° with the virion axis (*17*, *18*). In the diffraction-based model (*16*), a 180° flip about the $C^{\beta}-C^{\gamma}$ linkage is required to achieve compatibility with the experimental RLID and polarized Raman results. It is interesting to note that the spectroscopic measurements yield the same Trp 26 orientation whether the Ff particles are oriented either in solution by means of a velocity gradient (*18*) or in fibers by means of mechanical force (*17*). This implies that the change in state from solution to fiber and attendant changes in intervirion contacts and bulk solvent environment do not significantly affect the subunit conformation in the vicinity of Trp 26.

Recently, the RLID method was used to determine the orientations of Tyr 21 and Tyr 24 in flow-oriented Ff (*21*). Single-site Tyr → Met mutations in pVIII subunits of strain f1, designated f1(Y21M) and f1(Y24M), were employed to distinguish the UVRR signals of the two tyrosines. The RLID results indicate that the 2-fold axis of the phenolic ring of Tyr 21 is inclined at an angle of ∼40° and that of Tyr 24 is inclined at an angle of ∼44° from the virion axis. Although the orientation of Tyr 21 in the diffraction-based model (*13*, *16*) is close to the experimentally determined result, this is not the case for Tyr 24, where a rotation of ∼40° about the $C^{\alpha}-C^{\beta}$ bond is required to achieve consistency with the RLID experiment.

Here, we report the determination of the orientations of Tyr 21 and Tyr 24 side chains in the native Ff assembly using a novel experimental approach that is based upon polarized Raman microspectroscopy in combination with site-specific isotope labeling. Polarized Raman spectra have been collected on oriented fibers of the Y21M and Y24M mutants of strain f1, wherein deuterium labels have been incorporated at the $C^{\delta 1}$, $C^{\delta 2}$, $C^{\epsilon 1}$, and $C^{\epsilon 2}$ ring sites. The data are interpreted by using Raman tensors for the phenolic C−D stretching bands transferred from a single-crystal Raman analysis of the model compound, L-tyrosine-2,3,5,6-d_4. This approach permits exploitation of the C−D stretching region of the Raman spectrum (2200−2400 cm^{-1}), which is devoid of interference or overlap from any other Raman bands. Additionally, the C−D stretching modes are highly localized vibrations, and therefore, their Raman tensors are considered to be among the most reliable for transfer between the model compound (L-tyrosine) and the Ff target moieties (Tyr 21 and Tyr 24). In conjunction with the previous RLID study (*18*), the findings presented here provide a further basis for assessing whether local structure and environment in the central hydrophobic segment of the pVIII subunit are affected by the change in virion state from flow-oriented solution to mechanically oriented fiber.

MATERIALS AND METHODS

Sample Preparations. Wild-type fd was prepared from stocks obtained originally from L. A. Day (Public Health Research Institute, New York, NY). Mutants f1(Y21M) and f1(Y24M) were prepared from stocks obtained originally from G. Cesareni (Dipartimento di Biologia, Universita di Roma, Rome, Italy). Phage were grown on *E. coli* strain Hfr3300. Growth medium and standard reagents were obtained from Sigma Chemical (St. Louis, MO) and Fisher Scientific (St. Louis, MO). L-Tyrosine-2,3,5,6-d_4·HCl was obtained from Cambridge Isotope Laboratories (Woburn, MA).

Unlabeled viruses, fd, f1(Y21M), and f1(Y24M), were grown in MS medium containing 1% glucose and 4 mM $CaCl_2$. Mature viral particles, extruded through the bacterial cell membrane and into the growth medium, were collected by precipitation with poly(ethylene glycol) (20 g/L) and NaCl (0.5 M) followed by low-speed centrifugation (*15*). The virus precipitate was resuspended in 10 mM Tris (pH 7.8 ± 0.2) and pelleted by centrifugation at 330000*g* for 1.5 h at 4 °C. The resulting virus pellet was purified as described previously (*15*). A typical yield from a 1 L preparation of purified wild-type viral particles was 30−40 mg; that of purified mutant viral particles was 20 mg.

Three deuterium-labeled viruses were prepared: fd($2Y_{d4}$), f1(Y21M/$Y24_{d4}$), and f1(Y24M/$Y21_{d4}$). To incorporate L-tyrosine-2,3,5,6-d_4 into the virion coat, we employed M9 minimal growth medium, which contained the labeled amino acid at 0.1 mM per residue and all other amino acids at 0.1 mM each, with 10 μg/mL thiamine-HCl and 1% glucose. Labeled viruses were purified as described above. Typically, 20 mg of labeled fd and 10−15 mg of labeled f1 mutants were obtained from a 1 L preparation. Solutions of virus particles were drawn into oriented fibers for polarized Raman microspectroscopy as described previously (*17*, *19*).

Raman Microspectroscopy. The oriented fiber was sealed in a constant-relative humidity (92%) and constant-temperature (15 °C) chamber with the fiber axis (*c*) in the horizontal plane. Polarized Raman spectra were excited using the 514.5 nm line of a Coherent Innova 70 argon laser (Santa Clara, CA). The spectra were collected on a microspectrophotometer system consisting of an Olympus model BHSM microscope (Lake Success, NY), an ISA/Jobin Yvon model S3000 triple spectrograph (Edison, NJ), and an ISA Spectraview-2D charge-coupled-device detector, which has been described in detail previously (*25*).

The exciting radiation with electric vector polarized along the fiber axis (*c*) was directed onto the fiber through an 80× objective with a focal length of 15 mm. Raman scattering was collected with the same objective and directed through a polarizer to the monochromator. The polarizer permitted transmittance of only Raman scattering that was polarized along the same direction as that of the exciting radiation. By initially orienting the fiber axis parallel to the electric

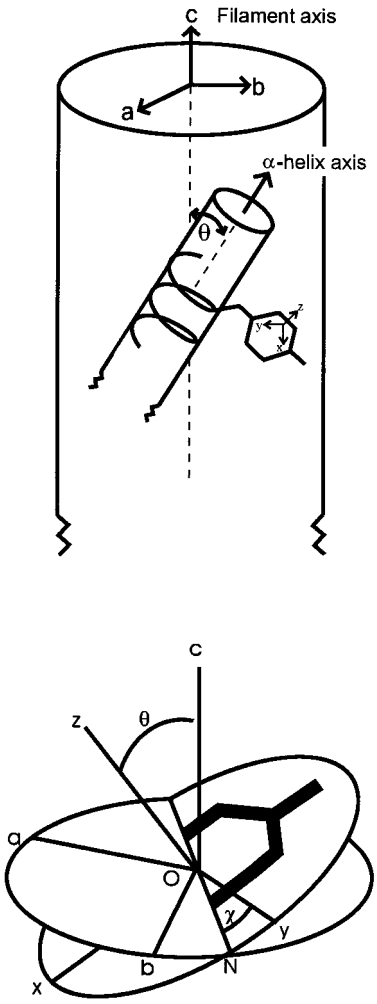

FIGURE 1: (Top) Coordinate system for the uniaxially oriented Ff fiber (*a*, *b*, *c*) in relation to the α-helical subunit and a tyrosine side chain. The drawing (not to scale) represents a small segment of the 880 nm virion and a few α-helical turns of one subunit. (Bottom) Eulerian angles θ and χ define the orientation of the coordinate system (*x*, *y*, *z*) for a tyrosine Raman tensor with respect to the (*a*, *b*, *c*) system. θ is the tilt angle (*c*−O−*z*) between the Raman tensor principal axis *z* and the fiber axis *c*. χ is the angle (*y*−O−N) formed by the Raman tensor principal axis *y* and the line of intersection between the plane (*ab*) normal to the fiber axis and the plane (*xy*) of the phenolic ring.

vector of the exciting radiation (which is also parallel to the electric vector of the scattered radiation), the *cc* spectrum (I_{cc}) was collected. Subsequently, upon rotation of the fiber axis by 90°, the *bb* spectrum (I_{bb}) was collected. Typically, three accumulations each of I_{cc} and I_{bb} were obtained with a detector integration time of 180 s each. The respective I_{cc} and I_{bb} accumulations were then averaged. This procedure was repeated five times, and the results were again averaged to produce the final I_{cc} and I_{bb} spectra. The disposition of the fiber with respect to its fixed coordinate system (*a*, *b*, *c*) is depicted in Figure 1 (top).

Raman tensors of phenolic C−D stretching modes are required for interpretation of the Raman polarization anisotropy of the $C^{\delta 1}$,$C^{\delta 2}$,$C^{\epsilon 1}$,$C^{\epsilon 2}$-tetradeuteriotyrosine moieties in labeled viruses. These tensors were obtained from a polarized Raman spectroscopic analysis of an oriented single crystal of L-tyrosine-2,3,5,6-d_4. The appropriate crystal was prepared and analyzed as described by detailed elsewhere (*26*).

Data Analysis. In the fiber-fixed coordinate system (*a*, *b*, *c*) of Figure 1 (top), the *c* axis is parallel to the virion axis, and axes *a* and *b* are equivalent and perpendicular to *c*. Also shown is a tyrosine side chain. A different coordinate system (*x*, *y*, *z*) is used to represent the tensor principal axes of each normal mode of vibration of the phenolic ring. The phenolic ring in question may correspond to either Tyr 21 or Tyr 24, depending upon the Ff variant under consideration. The (*x*, *y*, *z*) system for a given tyrosyl Raman band is generally unique, but because of virion symmetry, each is arranged symmetrically with respect to *c*. The orientation of each (*x*, *y*, *z*) system can be related to the Eulerian angles, θ and χ, as illustrated in Figure 1 (bottom) (*17*).

To each tyrosine normal mode (Raman band) we assign a Raman tensor $\boldsymbol{\alpha}$, which is defined as the first derivative of the molecular polarizability with respect to the vibrational normal coordinate. The tensor component α_{ij} represents the change in polarizability for radiation with incident and scattered electric vectors polarized, respectively, in the *i* and *j* directions. Here, we consider only the relative magnitudes of the principal (i.e., diagonal) tensor components, namely, $\alpha_{xx}/\alpha_{zz} \equiv r_1$ and $\alpha_{yy}/\alpha_{zz} \equiv r_2$ (*27*). Highly anisotropic Raman tensors are characterized with values of r_1 and/or r_2 differing greatly from unity, whereas isotropic tensors have $r_1 = r_2 = 1$. For Raman tensors that are axially symmetric with respect to *z*, $r_1 = r_2 \equiv r$ (*19*). Tensor components associated with any vibration can be calculated from knowledge of the appropriate polarized Raman band intensities I_{kl}, where *k* and *l* (=*a*, *b*, *c*) are the directions of the incident and scattered electric vectors, respectively (*28*).

For a local Raman tensor that is not symmetric along *z*, the polarized Raman intensity ratio I_{cc}/I_{bb} is given in terms of θ, χ, r_1, and r_2 by eq 1 (*17*, *29*).

$$I_{cc}/I_{bb} = 4[\sin^2\theta\,(r_1\cos^2\chi + r_2\sin^2\chi) + \cos^2\theta]^2/ [\cos^2\theta\,(r_1\cos^2\chi + r_2\sin^2\chi) + r_1\sin^2\chi + r_2\cos^2\chi + \sin^2\theta]^2 \quad (1)$$

We propose to use eq 1 to determine the phenolic ring orientation (θ, χ) in Ff by measuring the polarized Raman intensity ratios $(I_{cc}/I_{bb})^{I}$ and $(I_{cc}/I_{bb})^{II}$ of two specific Raman bands of the phenolic moiety (designated bands I and II), for which the corresponding Raman tensors (r_1^{I}, r_2^{I}) and (r_1^{II}, r_2^{II}) are known. Provided that the Raman tensors of bands I and II have a common *z* axis, a graphical solution for θ and χ is feasible. This is analogous to case V described previously by Tsuboi and co-workers (*17*), in determining the orientation of Trp 26. In effect, $(I_{cc}/I_{bb})^{I}$ is plotted as a contour line in $\theta^{I}-\chi^{I}$ space; $(I_{cc}/I_{bb})^{II}$ is plotted similarly in $\theta^{II}-\chi^{II}$ space, and an appropriate coordinate transformation (graphical superposition) is exploited to yield the unique θ and χ values common to data sets I and II. In the application described below, tyrosine bands I and II are those near 855 and 2282 cm^{-1}, respectively.

RESULTS

Figure 2 shows polarized Raman spectra (I_{cc} and I_{bb}) of oriented fibers of the unlabeled mutant f1 virions [f1(Y21M) and f1(Y24M)] in the spectral regions of 600−1100 and 1200−1700 cm^{-1}. As expected, the total Raman intensity

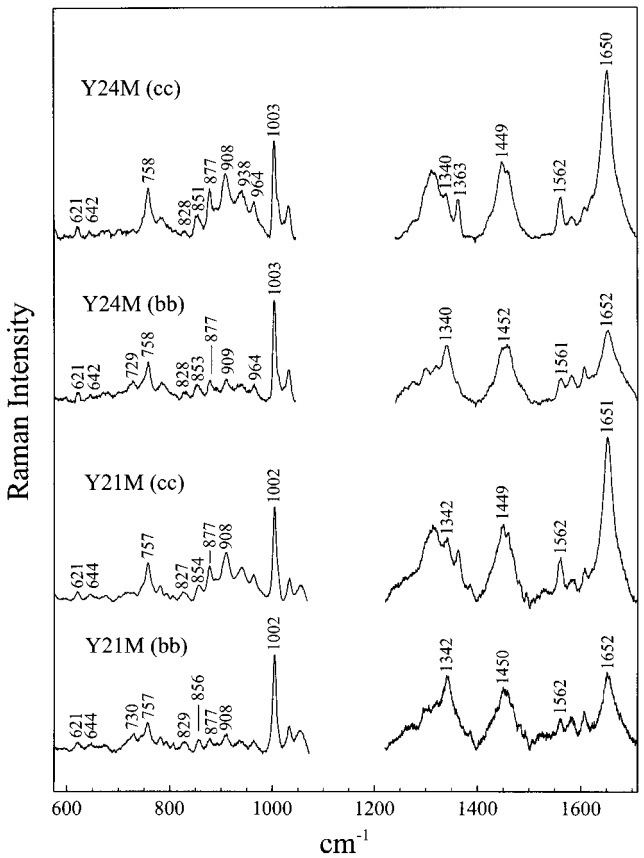

FIGURE 2: Polarized Raman spectra (I_{cc} and I_{bb}) of oriented fibers of the unlabeled mutant viruses f1(Y21M) and f1(Y24M) in the spectral regions of 600−1100 and 1200−1700 cm^{-1}. The data are reproducible to ±5% for independently drawn fibers. Raman intensities are normalized to the intensity of the isotropic marker band at 1002 cm^{-1} (Phe). The excitation wavelength is 514.5 nm.

($I_{cc} + I_{bb}$) of each tyrosine band in the Raman spectrum of each unlabeled f1 mutant is about half that of the corresponding band in the Raman spectrum of wild-type Ff (*19*). The f1 spectra are representative of the highest polarization ratios (I_{cc}/I_{bb}) that were obtained and indicate optimal virion alignment in the portion of the fiber exposed to the incident laser beam. The measured polarization ratios were also highly reproducible (within ±10%) from one fiber to another. In the comparison of I_{cc} and I_{bb}, intensities were normalized using the phenylalanine band at 1002 cm^{-1}, the intensity of which is independent of orientation.

Polarized Raman spectra in the region of 1500−2400 cm^{-1} of oriented fibers of deuterium-labeled mutant f1 virions [f1(Y21M/Y24$_{d4}$) and f1(Y24M/Y21$_{d4}$)] are shown in Figure 3. These data are characterized by the same reproducibility as those depicted in Figure 2. Intensity normalizations are based upon the phenylalanyl band at 1002 cm^{-1} for the region below 1800 cm^{-1} and the C−H stretching band complex (not shown) for the region above 2000 cm^{-1}.

A recent polarized Raman study of oriented single crystals of L-tyrosine and L-tyrosine-2,3,5,6-d_4 has provided Raman tensors for key vibrational modes of the phenolic moiety in the spectral region below 2000 cm^{-1} (*26*). The previous analysis is extended here to include the C−D stretching modes of the deuterated phenolic ring for application to the C$^{\delta1}$,C$^{\delta2}$,C$^{\epsilon1}$,C$^{\epsilon2}$-tetradeuteriotyrosine moieties in f1(Y21M/Y24$_{d4}$) and f1(Y24M/Y21$_{d4}$). Figure 4 shows representative polarized Raman spectra of the oriented single crystal of

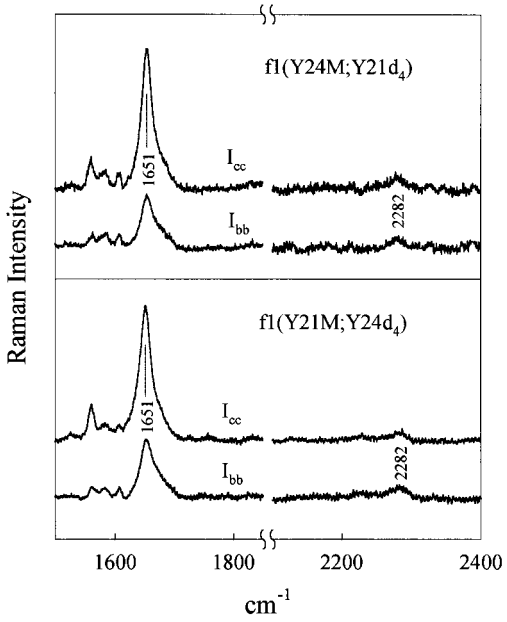

FIGURE 3: Polarized Raman spectra (I_{cc} and I_{bb}) of oriented fibers of the deuterium-labeled mutant viruses f1(Y21M/Y24$_{d4}$) and f1(Y24M/Y21$_{d4}$) in the spectral region of 1500−2400 cm^{-1}. Other conditions were as described in the legend of Figure 2.

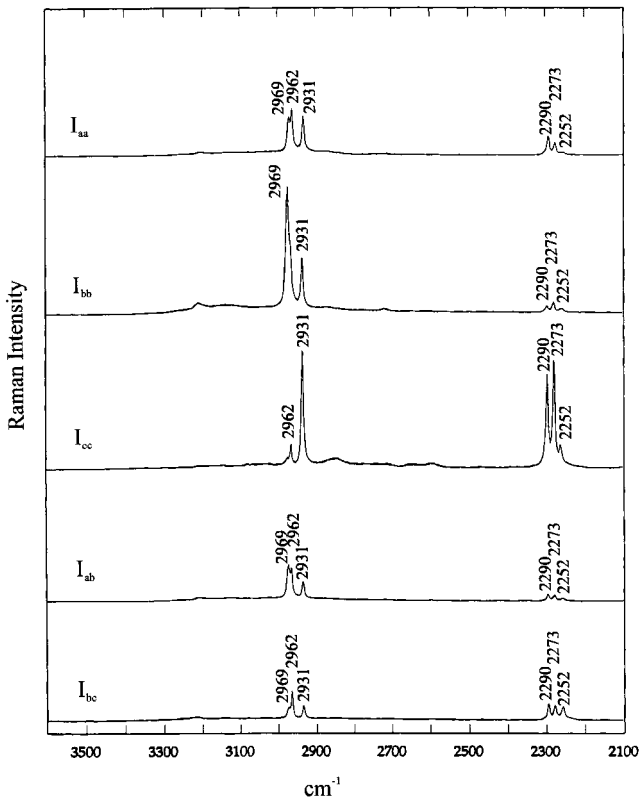

FIGURE 4: Polarized Raman spectra (I_{aa}, I_{bb}, I_{cc}, I_{ab}, and I_{bc}) in the region of 3500−2100 cm^{-1} of a single crystal of L-tyrosine-2,3,5,6-d_4. The instrumentation is described in ref *26*.

L-tyrosine-2,3,5,6-d_4 in the region above 2100 cm^{-1}, which displays the bands assigned to ring C−D stretching (2252, 2273, and 2290 cm^{-1}), exocyclic C$^{\alpha}$−H and H$^{\beta1}$−C$^{\beta}$−H$^{\beta2}$ stretching (2931, 2962, and 2969 cm^{-1}), and phenoxyl O−H stretching (3220 cm^{-1}) modes. Four normal modes are expected for the C−D stretching vibrations of L-tyrosine-2,3,5,6-d_4 (or for the pVIII C$^{\delta1}$,C$^{\delta2}$,C$^{\epsilon1}$,C$^{\epsilon2}$-tetradeuteriotyrosine moiety of each mutant). Two of the four are symmetric

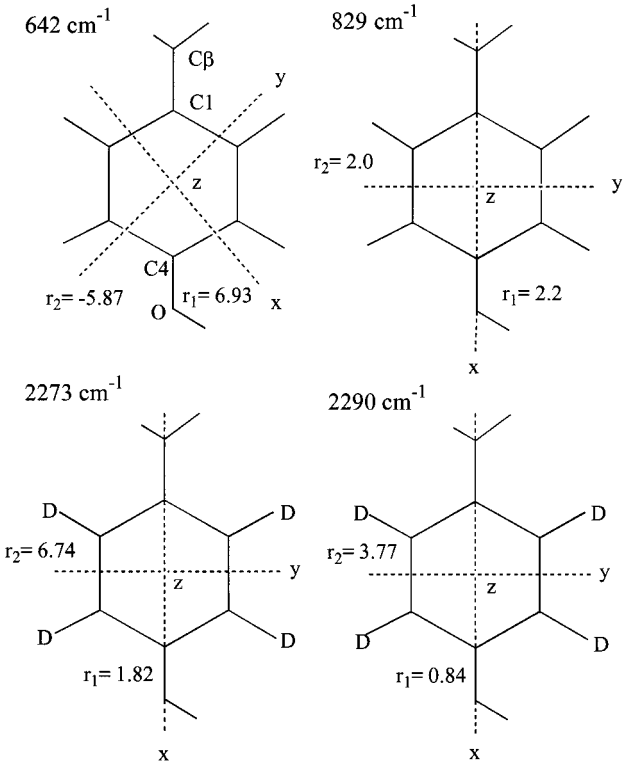

FIGURE 5: Raman tensors for bands of L-tyrosine at 642 and 829 cm^{-1} (top) and L-tyrosine-2,3,5,6-d_4 at 2273 and 2290 cm^{-1} (bottom). The former are assumed to be transferrable to the corresponding bands (near 644 and 855 cm^{-1}) of the unlabeled tyrosyl side chains of pVIII in mutant virions f1(Y21M) and f1(Y24M). Similarly, the latter are assumed to be transferable, after averaging, to the broad composite band (2282 cm^{-1}) of the labeled tyrosyl side chains of pVIII in f1(Y21M/$Y24_{d4}$) and f1(Y24M/$Y21_{d4}$). For each tensor, the local (*x*, *y*, *z*) coordinate system (see Figure 1) is indicated by the dashed lines for the *x* and *y* axes, with *z* perpendicular to the phenolic ring.

with respect to the pseudocenter of symmetry of the phenolic ring, and to these symmetric modes we assign the stronger Raman bands at 2273 and 2290 cm^{-1}. As seen in Figure 4, these bands are strong only for the I_{cc} measurement on L-tyrosine-2,3,5,6-d_4. This is explained by the fact that in the orthorhombic L-tyrosine crystal (space group $P2_12_12_1$), the phenolic ring plane is oriented nearly parallel to the crystallographic *bc* plane and the C^1-C^4 line is nearly collinear with respect to the crystallographic *b* axis. Therefore, it is evident that the polarizability oscillation for both the 2273 and 2290 cm^{-1} Raman bands takes place mainly along the direction perpendicular to the C^1-C^4 line and in the plane of the phenolic ring. Polarized Raman intensity ratios I_{aa}/I_{cc}, I_{bb}/I_{cc}, I_{ab}/I_{cc}, and I_{bc}/I_{cc} are 0.11, 0.10, 0.059, and 0.082, respectively, for the 2273 cm^{-1} band and 0.19, 0.070, 0.070, and 0.11, respectively, for the 2290 cm^{-1} band. From these data, Raman tensors for the two bands of L-tyrosine-2,3,5,6-d_4 at 2273 and 2290 cm^{-1} have been determined. The Raman tensors of present interest are shown in Figure 5.

DISCUSSION

Structure of the Ff Assembly: An Overview of Previous X-ray and Raman Results

Atomic coordinates of pVIII in the Ff assembly have been developed on the basis of molecular modeling and fiber X-ray diffraction data (*13*, *16*). In this model, the coordinates of the *k*th subunit are related to the coordinates of any given subunit ($k = 0$) by eq 2

$$\begin{bmatrix} x_k \\ y_k \\ z_k \end{bmatrix} = \begin{bmatrix} \cos R & -\sin R & 0 \\ \sin R & \cos R & 0 \\ 0 & 0 & 1 \end{bmatrix} \begin{bmatrix} x_0 \\ y_0 \\ z_0 \end{bmatrix} + \begin{bmatrix} 0 \\ 0 \\ P[k/5] \end{bmatrix} \quad (2)$$

where $R = (2\pi)(k/5) + (\tau)[k/5]$ and the term $[k/5]$ signifies the integral part of the ratio $k/5$. The helix parameters τ and P equal $-36°$ and 16.15 Å, respectively. The pVIII subunits are thus arranged as a left-handed five-start superhelix of C_5S_2 symmetry with 10 subunits per turn, wherein each subunit is modeled optimally as a continuous and slightly curved α-helix tilted by a small angle from the virion axis (*13*).

In previous Raman, polarized Raman, UVRR, and polarized UVRR (RLID) studies of Ff, key spectral bands were assigned and interpreted to confirm the subunit α-helical secondary structure, identify local conformations, environments, and interactions of side chains of pVIII and deoxynucleosides of packaged DNA, and demonstrate specific orientations of the subunit α-helix and selected aromatic side chains with respect to the virion axis (*14*, *15*, *17*−*24*, *30*). Although most of the Raman and X-ray results are in satisfactory agreement with one another, the spectroscopically determined indolyl (Trp 26) and phenolic (Tyr 24) ring orientations differ in detail from those of the proposed 1IFJ model. Specifically, the 1IFJ model requires an approximate 180° flip of the indolyl ring of Trp 26 (*17*, *18*) and a significant rotation about the $C^{\alpha}-C^{\beta}$ bond of Tyr 24 (*21*).

Structural Significance of the Results Presented Here

Subunit α-Helix Orientation. The amide I band of each mutant virion [f1(Y21M), f1(Y24M), f1(Y21M/$Y24_{d4}$), and f1(Y24M/$Y21_{d4}$)] is centered near 1651 cm^{-1} (Figures 2 and 3) and exhibits an I_{cc}/I_{bb} value in the range of 2.8 ± 0.2, which is within experimental error of the previously reported value of 3.01 ± 0.18 for wild-type Ff (*19*). [An exception is the f1(Y21M/$Y24_{d4}$) data set in the lower panel of Figure 3, for which $I_{cc}/I_{bb} \approx 2.4$, which can be attributed to a lower degree of uniaxial orientation in this particular sample (*31*).] Overall, the results presented here indicate an only marginally lower unidirectional orientation in fibers of Ff mutants, and confirm that the average α-helix tilt angle in mutant as in wild-type subunits is $16 \pm 4°$.

θ Values for Tyr 21 and Tyr 24 from Raman Scattering Anisotropy Near 855 cm^{-1}. For both f1(Y21M) and f1(Y24M), the tyrosyl Raman marker near 855 cm^{-1} exhibits a polarized Raman intensity ratio $(I_{cc}/I_{bb})^{855}$ of 1.6 ± 0.1 (Figure 2). The assignment and structural significance of the 855 cm^{-1} marker have been considered in detail elsewhere (*14*). Here, we use the value of $(I_{cc}/I_{bb})^{855}$ to assess the phenolic ring orientation of the unique tyrosine of each f1 mutant. For this purpose, we assume that the Raman tensor for the band near 855 cm^{-1} can be approximated by that of the corresponding Raman marker (829 cm^{-1}) of L-tyrosine. The latter, which is shown in Figure 5, has been determined experimentally by polarized Raman analysis of an L-tyrosine single crystal and theoretically by ab initio molecular orbital calculations on L-tyrosine (*26*). When $r_1 = 2.2$ and $r_2 = 2.0$, we obtain by using eq 1 the solid contour lines of Figure 6,

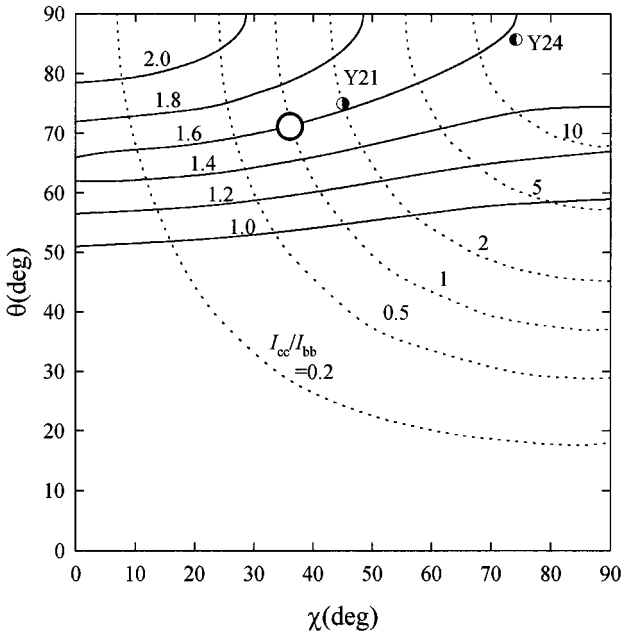

FIGURE 6: Contours of I_{cc}/I_{bb} in $\theta-\chi$ space for Raman bands of f1 mutant viruses near 855 (—) and 2282 cm^{-1} (- - -). The large open circle at the intersection of the $(I_{cc}/I_{bb})^{855} = 1.6$ and $(I_{cc}/I_{bb})^{2282} = 1.0$ contours represents the Eulerian coordinates ($\theta = 71°$, $\chi = 36°$) and defines the Tyr 21 and Tyr 24 orientations in Ff that are consistent with the polarized Raman spectra. The half-shaded circles indicate the coordinates proposed for Tyr 21 and Tyr 24 in the Ff model of Marvin and co-workers (Protein Data Bank entry 1IFJ) (*16*).

which express $(I_{cc}/I_{bb})^{855}$ as a parametric function of the Eulerian coordinates θ and χ (Figure 1). Both the Tyr 21 residue of f1(Y24M) and the Tyr 24 residue of f1(Y21M) are characterized by the same parametric relationship between $(I_{cc}/I_{bb})^{855}$ and θ and χ. The appropriate contour line of Figure 6 [i.e., $(I_{cc}/I_{bb})^{855} = 1.6$] indicates that the corresponding value of θ for each mutant will fall within the narrow range of 65−90°, although χ may fall within the broader range of 0−74°. Wild-type Ff also exhibits an $(I_{cc}/I_{bb})^{855}$ of 1.6 ± 0.1, indicating the same average θ and χ values as for the f1 mutants (*17*).

The molecular model (1IFJ) proposed for wild-type Ff assumes θ values for Tyr 21 and Tyr 24 of 75° and 85°, respectively (*13*), consistent with the experimental Raman scattering anisotropies near 855 cm^{-1}. Therefore, both diffraction-based model building and polarized Raman spectroscopy indicate that the normals to the phenolic ring planes are close to perpendicular to the fiber axis; i.e., the plane of each phenolic ring is close to parallel to the fiber axis. To further specify the ring orientations, and narrow the allowable range for χ, we consider the polarization anisotropy at 2282 cm^{-1}, as discussed next.

χ Values for Tyr 21 and Tyr 24 from Raman Scattering Anisotropy Near 2282 cm^{-1}. The Ff variant fd($2Y_{d4}$) exhibits a Raman band near 2282 cm^{-1}, which can be assigned to the symmetrical C−D stretching modes (components at 2273 and 2290 cm^{-1}) of the deuterium-labeled $C^{\delta 1}$, $C^{\delta 2}$, $C^{\epsilon 1}$, and $C^{\epsilon 2}$ sites (*15*). Although the 2282 cm^{-1} band is relatively weak, it is isolated from all other vibrational modes of the protein and DNA constituents of the virion and is thus well suited to Raman scattering anisotropy measurement. Using tensors (Figure 5) obtained from polarized Raman analysis of L-tyrosine-2,3,5,6-d_4 (Figure 4), we here interpret the $(I_{cc}/I_{bb})^{2282}$ values for residue Tyr 21 of f1(Y24M/$Y21_{d4}$) and residue Tyr 24 of f1(Y21M/$Y24_{d4}$).

Polarized Raman spectra of f1(Y24M/$Y21_{d4}$) and f1(Y21M/$Y24_{d4}$) are shown in Figure 3. Despite the modest signal-to-noise level of the data, it is clear that the value of $(I_{cc}/I_{bb})^{2282}$ is close to unity for each f1 variant. A conservative estimate of the uncertainty in $(I_{cc}/I_{bb})^{2282}$ is 30%; i.e., $(I_{cc}/I_{bb})^{2282} = 1.0 \pm 0.3$ for both f1(Y24M/$Y21_{d4}$) and f1(Y21M/$Y24_{d4}$). We also measured the $(I_{cc}/I_{bb})^{2282}$ value on four oriented fibers of fd($2Y_{d4}$) (data not shown), wherein $C^{\delta 1}$,$C^{\delta 2}$,$C^{\epsilon 1}$,$C^{\epsilon 2}$-tetradeuteriotyrosine is incorporated at both positions 21 and 24 of pVIII. As expected, the total C−D Raman intensity $[(I_{cc} + I_{bb})^{2282}]$ for fd($2Y_{d4}$) is twice that observed for either f1 mutant in Figure 4. The fd($2Y_{d4}$) fibers also exhibited the same amide I Raman scattering anisotropy as unlabeled fd [i.e., $(I_{cc}/I_{bb})^{1651} = 3.0$, indicating the same high degree of unidirectional orientation], and the same Raman scattering anisotropy at 2282 cm^{-1} as for the labeled mutants [i.e., $(I_{cc}/I_{bb})^{2282} = 1.0$, confirming the same phenolic ring orientations]. The higher signal-to-noise ratio at 2282 cm^{-1} in fd($2Y_{d4}$) allows refinement of the uncertainty in $(I_{cc}/I_{bb})^{2282}$ to less than 20%.

To interpret the $(I_{cc}/I_{bb})^{2282}$ measurements on f1(Y24M/$Y21_{d4}$), f1(Y21M/$Y24_{d4}$), and fd($2Y_{d4}$), we assume that Raman tensors of the 2273 and 2290 cm^{-1} bands of L-tyrosine-2,3,5,6-d_4 (Figure 5, bottom) may be combined to yield an effective Raman tensor for the composite 2282 cm^{-1} band of each Ff variant. This assumption is supported by the fact that the shapes of the Raman tensors for the 2273 and 2290 cm^{-1} modes are very similar to one another and are defined in terms of the same (x, y, z) coordinate system, as seen in Figure 5. Accordingly, when $\langle r_1 \rangle = 1.33$ and $\langle r_2 \rangle = 5.26$, we obtain by using eq 1 the contours shown as dashed lines in Figure 6, which express $(I_{cc}/I_{bb})^{2282}$ as a parametric function of θ and χ. The only values of θ and χ in Figure 6 that are compatible with both the polarized Raman intensity measurements at 855 cm^{-1} (solid contours) and 2282 cm^{-1} (dashed contours) are those at the intersection of the $(I_{cc}/I_{bb})^{855} = 1.6$ and $(I_{cc}/I_{bb})^{2282} = 1.0$ contours, namely, $(\theta, \chi)^{Y21} = (\theta, \chi)^{Y24} = (71 \pm 5°, 36 \pm 5°)$. Thus, we conclude that both Tyr 21 and Tyr 24 are oriented similarly with respect to the fiber axis, such that the normal to the phenolic ring plane is close to perpendicular to the fiber axis, and the phenolic C^1-C^4 line forms an angle of about 36° with the O−N line in Figure 1. These results apply to both tyrosines of wild-type Ff (fd) and the single tyrosine of each f1 mutant.

Consistency with Raman Scattering Anisotropy at 644 cm^{-1}. The Raman marker of tyrosine at 644 cm^{-1} is relatively weak. However, it is largely devoid of overlap from other vibrational bands in Raman spectra of wild-type Ff, mutant f1, and deuterium-labeled variants (*15*). Therefore, it is of interest to assess whether the Raman scattering anisotropy at 644 cm^{-1} [$1.2 < (I_{cc}/I_{bb})^{644} < 2.5$ (Figure 2)] is consistent with the tyrosine orientations determined above. Although the Raman tensor for the 644 cm^{-1} mode (Figure 5, upper left) has a principal axis system different from that of the 829 cm^{-1} mode (Figure 5, upper right), the two tensors share a common z axis, and a 45° rotation of the former with respect to the latter allows comparison with the data depicted in Figure 6. Taking this into account, we find that an oriented Ff fiber containing a tyrosine residue with Eulerian coordi-

Table 1: Revised Atomic Coordinates of the Phenolic Moieties of Tyr 21 and Tyr 24 of the Ff Subunit

tyrosine 21[a]					tyrosine 24[b]				
atom	(*N*)	*x*	*y*	*z*	atom	(*N*)	*x*	*y*	*z*
C^{γ}	(145)	0.022	−21.412	44.262	C^{γ}	(169)	−0.267	−24.098	39.195
$C^{\delta 1}$	(146)	−1.349	−21.501	44.117	$C^{\delta 1}$	(170)	0.497	−25.332	39.057
$C^{\delta 2}$	(147)	0.561	−21.626	45.540	$C^{\delta 2}$	(171)	−0.798	−23.882	40.459
$C^{\epsilon 1}$	(148)	−2.165	−21.846	45.191	$C^{\epsilon 1}$	(172)	0.662	−26.183	40.113
$C^{\epsilon 2}$	(149)	−0.236	−21.983	46.620	$C^{\epsilon 2}$	(173)	−0.636	−24.735	41.549
C^{ζ}	(150)	−1.605	−22.079	46.454	C^{ζ}	(174)	0.105	−25.917	41.366
O	(151)	−2.371	−22.605	47.478	O	(175)	0.294	−26.772	42.423

[a] Obtained from the atomic coordinates of atoms 145−151 of entry 1IFJ of the Protein Data Bank (*13*) by rotating 10° about the $C^{\alpha}-C^{\beta}$ bond. [b] Obtained from the atomic coordinates of atoms 169−175 of entry 1IFJ of the Protein Data Bank (*13*) by rotating 50° about the $C^{\alpha}-C^{\beta}$ bond and 20° about the $C^{\beta}-C^{\gamma}$ bond.

nates (71°, 36°) should exhibit an $(I_{cc}/I_{bb})^{644}$ of 1.9. Thus, the observed $(I_{cc}/I_{bb})^{644}$ results are consistent with those discussed above.

Comparison with RLID and Model-Building Results

If we define ψ as the angle of inclination of the phenolic C^1-C^4 line from the *virion axis*, the present θ and χ values of 71 ± 5° and 36 ± 5°, respectively, correspond to a ψ of 41 ± 5°. This is in agreement with the results obtained in RLID measurements on flow-oriented solutions of the same f1 mutants (*21*), where it was found that $\psi = 39.5 \pm 1.4°$ for Tyr 21 and $\psi = 43.7 \pm 0.6°$ for Tyr 24.

Values of θ and χ for Tyr 21 and Tyr 24 in the fiber X-ray diffraction-based model can be calculated from atomic coordinates for Ff in Protein Data Bank entry 1IFJ. $(\theta, \chi)^{Y21} = (75°, 45°)$ for Tyr 21, and $(\theta, \chi)^{Y24} = (85°, 74°)$ for Y24. These coordinates, which are indicated by half-filled circles in the contour map of Figure 6, show that the orientation of Tyr 21 in the 1IFJ model is reasonably close to that determined by polarized Raman (and RLID) measurements, whereas that of Tyr 24 differs greatly from the experimental results. In fact, if the value of χ for Tyr 24 were to be as high as 74° (1IFJ model), then the polarized Raman intensity ratio for the 2282 cm^{-1} band of Figure 3 would have to be as great as 10, which is well outside the uncertainties of experimental measurements on f1(Y21M/$Y24_{d4}$) $[(I_{cc}/I_{bb})^{2282} = 1.0 \pm 0.3]$ and fd($2Y_{d4}$) $[(I_{cc}/I_{bb})^{2282} = 1.0 \pm 0.2]$.

Atomic Coordinates of Tyr 21 and Tyr 24

As noted above, the present polarized Raman intensity measurements on oriented Ff fibers [i.e., $(I_{cc}/I_{bb})^{855}$, $(I_{cc}/I_{bb})^{2282}$, and $(I_{cc}/I_{bb})^{644}$] as well as earlier RLID measurements on flow-oriented Ff solutions (*21*) both indicate Tyr 21 and Tyr 24 orientations for which θ and χ equal 71° and 36°, respectively. A previously proposed model [Protein Data Bank entry 1IFJ (*13*)] differs somewhat from these experimental results. However, rotation of the phenolic moiety of Tyr 21 by 10° about the $C^{\alpha}-C^{\beta}$ axis and rotations of the phenolic moiety of Tyr 24 by 50° about the $C^{\alpha}-C^{\beta}$ axis and by 20° about the $C^{\beta}-C^{\gamma}$ axis would bring the tyrosine orientations of the proposed 1IFJ model into consistency with the Raman measurements. The atomic coordinates corresponding to such refined tyrosine orientations are listed in Table 1.

An energy minimization of the refined 1IFJ model in the context of the Ff capsid (25 subunits of the five-start helical assembly defined by eq 2) was carried out using the X-PLOR program (*32*). Figure 7 shows the optimized structure for neighboring subunits of the capsid. Tyrosines in this subunit structure are characterized by side chain torsions that are within the standard ranges of Ponder and Richards (*33*) ($\chi^1 = -68$ and $\chi^2 = -71$ for Tyr 21, and $\chi^1 = -47$ and $\chi^2 = -31$ for Tyr 24).

In recent work, Welsh and co-workers (*34*) observed that a coat protein mutation can alter the helical symmetry of subunit packing in the Ff capsid. For example, the standard or "canonical" symmetry in strain M13 (Protein Data Bank entry 1IFI) is replaced by the "diad" helix symmetry in strains fd and f1 (1IFJ). The subunit of M13 differs from that of f1 or fd only at position 12, where Asn is in lieu of Asp. Similarly, the Y21M mutation in the f1 subunit converts the diad symmetry of the wild-type assembly (1IFJ) to the canonical symmetry (1IFI). Interestingly, however, residues Tyr 21 and Tyr 24 exhibit virtually identical side chain orientations in the 1IFJ and 1IFI models (*13*, *34*). Accordingly, differences in helical symmetry between models 1IFJ and 1IFI are not expected to impact significantly upon the tyrosine side chain orientations investigated here.

Effect of the Tyr 24 → Met Mutation on Raman Markers of Trp 26

Figure 2 shows that in the spectrum of f1(Y21M) the polarized Raman intensity ratio for the Trp 26 marker at 757 cm^{-1} $[(I_{cc}/I_{bb})^{757}]$ is 1.6. The same value is observed for wild-type fd (*17*). However, for f1(Y24M), we find $(I_{cc}/I_{bb})^{758} = 1.2$. Thus, it appears that the Y24M mutation (but not the Y21M mutation) leads to a modest change in the orientation of Trp 26. On the other hand, both mutants, as well as wild-type fd, exhibit similar I_{cc}/I_{bb} values for the 1560 cm^{-1} marker, namely, $(I_{cc}/I_{bb})^{1560} = 2.8 \pm 0.5$. This indicates a similar indolyl orientation (including $|\chi^{2,1}|$ torsion) in all Ff variants.

We interpret these results as evidence that the Trp 26 indolyl ring is oriented slightly differently in f1(Y24M) than in either wild-type fd or f1(Y21M), and that this effect cannot be attributed simply to a difference in $|\chi^{2,1}|$. As shown previously, the 1560 cm^{-1} vibration has its greatest polarizability oscillation along the pseudo-2-fold axis of the indolyl ring, whereas for the 757 cm^{-1} vibration, the polarizability oscillation is greatest along the perpendicular in-plane direction (see ref *17* and citations therein). Assuming that these tensors retain their respective characters in all Ff variants, we may be conclude that the indolyl ring of Trp 26 in the f1(Y24M) variant is rotated slightly with respect to its pseudo-2-fold axis from the orientation preferred in wild-type fd (possibly due to a change in the side chain

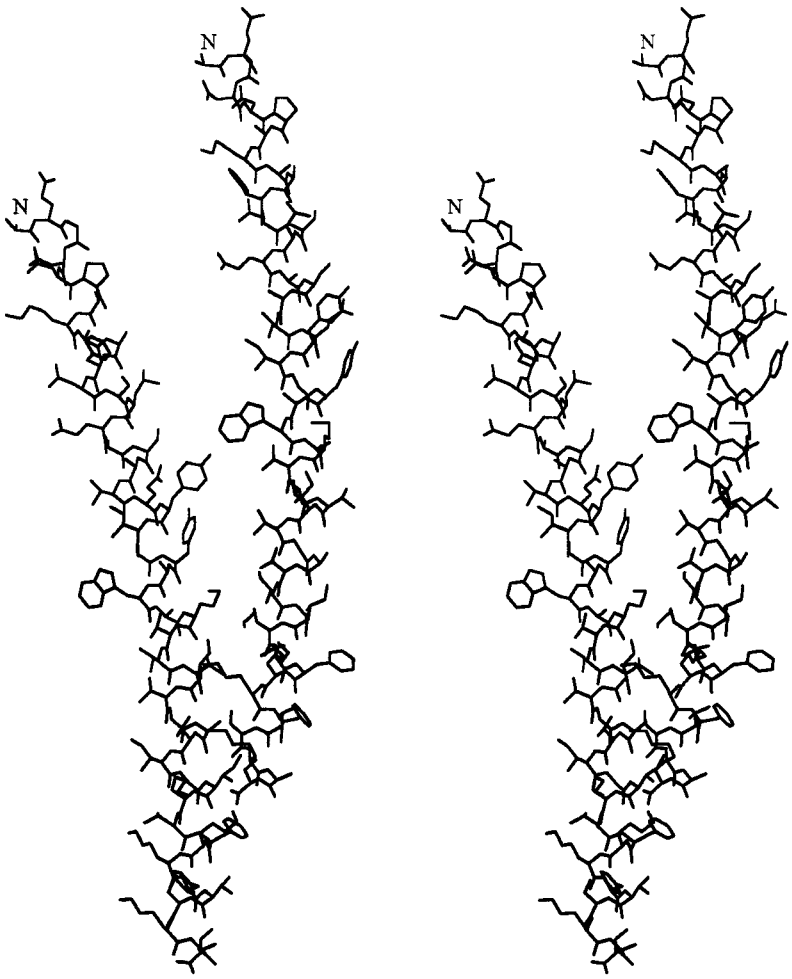

FIGURE 7: Stereodiagram of the energy-minimized structure of neighboring subunits ($k = 0$ and $k = 5$) in the assembly model proposed here for the Ff capsid. The energy minimization was carried out using the X-PLOR program (*32*) on 25 consecutively indexed subunits, with the coordinates for Tyr 21 and Tyr 24 developed from the results presented here and coordinates for other residues obtained as previously described (*13*, *16*, *17*, *19*, *37*). The virion axis runs vertically, and the subunit N-termini are at the top.

torsion χ^1). The magnitude of the rotation corresponding to the observed change in $(I_{cc}/I_{bb})^{757}$ is estimated to be about 20° along θ and essentially 0° along χ. The direction of the indolyl pseudo-2-fold axis presumably undergoes no significant change in this process.

We have used the 1IFJ subunit structure (modified as shown in Figure 7) to evaluate whether an assembly model generated by eq 2 could account for the observed effect of the Y24M mutation on Raman markers of Trp 26. For a given subunit (index $k = 0$), the nearest neighbors are those indexed by k values of ±5, ±6, ±11, and ±17 (*13*). Extension of the model of Figure 7 to include all near neighbors shows that none is likely to account for a *direct* Tyr 24−Trp 26 contact. We conclude that reorientation of the Trp 26 indole by the Y24M mutation is not due to a direct Tyr 24−Trp 26 contact, but presumably reflects a less localized effect involving additional side chains at the subunit interface. The putative side chains cannot be identified from the Raman spectra.

DNA Base Orientations Are Nonrandom and Invariant to the Tyrosine Mutations

The polarized Raman spectra of f1(Y21M) exhibit sufficiently high signal-to-noise ratios to permit meaningful measurement of polarization anisotropy in weak bands assigned to vibrations of the bases of packaged Ff DNA. The DNA bases contribute predominantly, if not completely, to the Raman markers at 675 (dG), 730 (dA), 745 (dT), 782 (dC) and ~1475 cm^{-1} (dG and dA) (*24*, *30*, *35*). Interestingly, several of these bands exhibit I_{cc}/I_{bb} values differing from unity, an indication that the DNA bases are not oriented randomly. This is evident in Figure 2 for the adenine band at 730 cm^{-1} and for the composite purine band at 1475 cm^{-1}, for both of which $I_{bb} > I_{cc}$. The same results have been found for wild-type Ff (*17*). These results imply that the long axes of the adenine and guanine rings are aligned closer to perpendicular than to parallel to the virion axis. Because dA and dG are distributed throughout the viral genome, such preferred base orientations presumably occur along the entire DNA−protein interface. In addition, the tyrosine mutations do not alter the polarization anisotropy of the DNA vibrations, which further confirms that the Tyr 21 and Tyr 24 side chains are not in contact with packaged DNA.

SUMMARY AND CONCLUSIONS

Phenolic ring orientations of tyrosine residues (Tyr 21 and Tyr 24) in the capsid subunit (pVIII) of filamentous bacteriophage Ff have been determined by polarized Raman microspectroscopy of oriented virion fibers. The experiments were carried out on Ff variants carrying single-site tyrosine

mutations in pVIII. These are the same Ff variants that have been examined by fiber X-ray diffraction and solid-state NMR analyses (*13*, *31*). The polarized Raman approach has been made feasible for this structural analysis by exploiting Raman marker bands of vibrations localized in $C^{\delta 1}$,$C^{\delta 2}$,$C^{\epsilon 1}$,$C^{\epsilon 2}$-tetradeuteriotyrosyl moieties incorporated into pVIII of the native assembly. The Raman tensors required for interpretation of the polarization anisotropy of Raman C−D stretching bands were transferred from L-tyrosine-2,3,5,6-d_4.

Phenolic ring orientations determined here for the Ff fiber are, within experimental uncertainty, identical to those determined by Raman linear intensity difference spectroscopy of Ff in solution (*18*). Accordingly, any differences between fiber and solution in detailed solvent and intervirion contacts do not affect local subunit geometry in the vicinity of positions 21 and 24 of the pVIII sequence. This extends the previous similar finding for the indolyl ring of position 26 (*17*, *18*). Evidently, the central hydrophobic segment of pVIII is well protected from solvent contact and well insulated from structural polymorphism required for filament flexibility. The flexible nature of the Ff filament presumably originates from a greater potential for structural polymorphism in the N- and C-terminal regions.

The mutation of either Tyr 21 or Tyr 24 to Met produces no change in the high α-helicity of the pVIII subunit and no change in the angular displacement (∼16°) of the subunit α-helix axis with respect to the virion axis. The tyrosine mutations also generate no significant changes to the Raman markers that are diagnostic of deoxynucleoside conformation. These results are consistent with the notion that the entire central hydrophobic segment of pVIII (residues 21−39) serves as a hydrophobic "core" in the assembled capsid, more important for defining and stabilizing intersubunit contacts than for facilitating subunit−solvent or subunit−DNA contacts. It is interesting to note that the Raman signatures of both pVIII tyrosines lack the canonical Fermi doublet (couplet at 830 and 850 cm^{-1}) that is diagnostic of phenoxyl hydrogen bonding and yield instead a singlet Raman marker near 855 cm^{-1} (*14*). Very recent work indicates that such a Raman signature demonstrates the absence of significant hydrogen bonding interaction of the tyrosyl O−H group (*36*). The conservation of subunit orientation and secondary structure despite relatively nonconservative Tyr → Met mutations is in accord with the notion that phenoxyl groups of Tyr 21 and Tyr 24 do not make key hydrogen bonding contributions to the Ff assembly. This is also entirely consistent with the proposed solvent inaccessibility of the central hydrophobic core of pVIII.

The Tyr 24 → Met mutation perturbs, albeit slightly, the Raman signature of Trp 26 in the Ff capsid. A pVIII molecular model based upon the Raman and X-ray diffraction data (Figure 7) suggests, however, that the Tyr 24 side chain is not in direct contact with the Trp 26 side chain of any other subunit in the Ff capsid. This implies either a need for revision of the 1IFJ assembly model or that perturbation of the Trp 26 environment is transmitted indirectly through readjustment of one or more other side chains in the hydrophobic core.

ACKNOWLEDGMENT

We thank Ms. Olivia Osman (University of Missouri−Kansas City) and Dr. Arantxa Rodriguez-Casado (University of Missouri−Kansas City) for preparation and purification of mutant and deuterium-labeled f1 phages and Ms. Mika Suzuki (Iwaki-Meisei University) for recording the polarized Raman spectra of L-tyrosine-d_4 single crystals.

REFERENCES

1. Denhardt, D. T., Dressler, D., and Ray, D. S. (1978) *The Single-Stranded DNA Phages*, Cold Spring Harbor Laboratory Press, Cold Spring Harbor, NY.
2. Day, L. A., Marzec, C. J., Reisberg, S. A., and Casadevall, A. (1988) *Annu. Rev. Biophys. Biophys. Chem. 17*, 509−539.
3. Webster, R. E. (1996) in *Phage Display of Peptides and Proteins* (Kay, B. K., Winter, J., and McCaffery, J., Eds.) pp 1−20, Academic Press, London.
4. Marvin, D. A. (1998) *Curr. Opin. Struct. Biol. 8*, 150−158.
5. Thomas, G. J., Jr., and Murphy, P. (1975) *Science 188*, 1205−1207.
6. Opella, S. J., Cross, T. A., DiVerdi, J. A., and Sturm, C. F. (1980) *Biophys. J. 80*, 531−548.
7. Thomas, G. J., Jr., Prescott, B., and Day, L. A. (1983) *J. Mol. Biol. 165*, 321−356.
8. Cross, T. A., Tsang, P., and Opella, S. J. (1983) *Biochemistry 22*, 721−726.
9. Clack, B. A., and Gray, D. M. (1989) *Biopolymers 28*, 1861−1873.
10. Clack, B. A., and Gray, D. M. (1992) *Biopolymers 32*, 795−810.
11. Arnold, G. E., Day, L. A., and Dunker, A. K. (1992) *Biochemistry 31*, 7948−7956.
12. Glucksman, M. J., Bhattacharjee, S., and Makowski, L. (1992) *J. Mol. Biol. 226*, 455−470.
13. Marvin, D. A., Hale, R. D., Nave, C., and Citterich, M. H. (1994) *J. Mol. Biol. 235*, 260−286.
14. Overman, S. A., Aubrey, K. L., Vispo, N. S., Cesareni, G., and Thomas, G. J., Jr. (1994) *Biochemistry 33*, 1037−1042.
15. Overman, S. A., and Thomas, G. J., Jr. (1995) *Biochemistry 34*, 5440−5451.
16. Symmons, M. F., Welsh, L. C., Nave, C., Marvin, D. A., and Perham, R. N. (1995) *J. Mol. Biol. 245*, 86−91.
17. Tsuboi, M., Overman, S. A., and Thomas, G. J., Jr. (1996) *Biochemistry 35*, 10403−10410.
18. Takeuchi, H., Matsuno, M., Overman, S. A., and Thomas, G. J., Jr. (1996) *J. Am. Chem. Soc. 118*, 3498−3507.
19. Overman, S. A., Tsuboi, M., and Thomas, G. J., Jr. (1996) *J. Mol. Biol. 259*, 331−336.
20. Overman, S. A., and Thomas, G. J., Jr. (1998) *J. Raman Spectrosc. 29*, 23−29.
21. Matsuno, M., Takeuchi, H., Overman, S. A., and Thomas, G. J., Jr. (1998) *Biophys. J. 74*, 3217−3225.
22. Overman, S. A., and Thomas, G. J., Jr. (1998) *Biochemistry 37*, 5654−5665.
23. Overman, S. A., and Thomas, G. J., Jr. (1999) *Biochemistry 38*, 4018−4027.
24. Wen, Z. Q., Armstrong, A., and Thomas, G. J., Jr. (1999) *Biochemistry 38*, 3148−3156.
25. Thomas, G. J., Jr., Benevides, J. M., Overman, S. A., Ueda, T., Ushizawa, K., Saitoh, M., and Tsuboi, M. (1995) *Biophys. J. 68*, 1073−1086.
26. Tsuboi, M., Ezaki, Y., Aida, M., Suzuki, M., Yimit, A., Ushizawa, K., and Ueda, T. (1998) *Biospectroscopy 4*, 61−71.
27. Tsuboi, M., and Thomas, G. J., Jr. (1997) *Appl. Spectrosc. Rev. 32*, 263−269.
28. Benevides, J. M., Tsuboi, M., Wang, A. H.-J., and Thomas, G. J., Jr. (1993) *J. Am. Chem. Soc. 115*, 5351−5359.
29. Tsuboi, M., Ikeda, T., and Ueda, T. (1991) *J. Raman Spectrosc. 22*, 619−626.
30. Wen, Z. Q., Overman, S. A., and Thomas, G. J., Jr. (1997) *Biochemistry 36*, 7810−7820.

31. Tan, W. M., Jelinek, R., Opella, S. J., Malik, P., Terry, T. D., and Perham, R. N. (1999) *J. Mol. Biol. 286*, 787−796.
32. Brünger, A. T. (1992) *X-PLOR*, version 3.1, Yale University Press, New Haven, CT.
33. Ponder, J. W., and Richards, F. M. (1987) *J. Mol. Biol. 193*, 775−791.
34. Welsh, L. C., Symmons, M. F., Nave, C., Perham, R. N., Marseglia, E. A., and Marvin, D. A. (1996) *Macromolecules 29*, 7075−7083.
35. Wen, Z. Q., and Thomas, G. J., Jr. (1998) *Biopolymers 45*, 247−256.
36. Arp, Z., Laane, J., Overman, S. A., and Thomas, G. J., Jr. (2001) *Biochemistry* (in press).
37. Aubrey, K. L., and Thomas, G. J., Jr. (1991) *Biophys. J. 61*, 1337−1349.

BI001936N